

# Catalytic C–H Trifluoromethylation of Arenes and Heteroarenes via Visible Light Photoexcitation of a Co(III)–CF<sub>3</sub> Complex

Christopher S. Kuehner,<sup>a</sup> Andrew G. Hill,<sup>a</sup> Caleb F. Harris,<sup>a</sup>  
Christian A. Owens,<sup>a</sup> John Bacsa,<sup>a,b</sup> and Jake D. Soper<sup>\*,a</sup>

<sup>a</sup>School of Chemistry and Biochemistry, Georgia Institute of Technology,  
Atlanta, Georgia 30332-0400, United States

<sup>b</sup>X-ray Crystallography Center, Department of Chemistry, Emory University,  
1515 Dickey Drive, Atlanta, Georgia 30322, United States

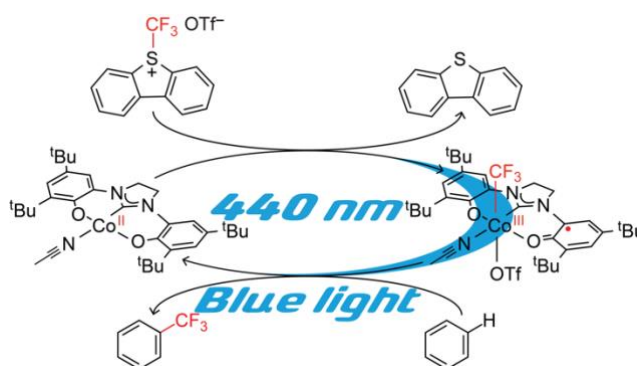
Email: jake.soper@gatech.edu

## Abstract:

A cobalt photocatalyst for direct trifluoromethylation of (hetero)arene C(sp<sup>2</sup>)–H bonds is described and shown to operate via visible light activation of a Co–CF<sub>3</sub> intermediate, which functions as a combined chromophore and organometallic reaction center. Chemical oxidations of previously reported (OCO)Co complexes containing a redox-active [OCO] pincer ligand afford a Co–CF<sub>3</sub> complex two oxidation states above Co(II). Computational and spectroscopic studies, are consistent with formulation of the product as [(OCO•)Co<sup>III</sup>(CF<sub>3</sub>)(THF)(OTf)] (**II**) containing an open-shell [OCO•]<sup>1-</sup> radical ligand bound to a S = 0 Co(III) center. **II** is thermodynamically stable, but exposure to blue (440 nm) light induces Co–CF<sub>3</sub> bond homolysis and release of •CF<sub>3</sub>, which is trapped by radical acceptors including TEMPO•, (hetero)arenes, or the radical [OCO•] ligand in **II**. The latter comprises a competitive degradation pathway, which is overcome under catalytic conditions using excess substrate. Accordingly, generation of **II** from the reaction of [(OCO)Co<sup>II</sup>L] (**III**) (L = THF, MeCN) with Umemoto's dibenzothiophenium trifluoromethylating reagent (**1**) followed by photolytic Co–CF<sub>3</sub> bond activation completes

a photoredox catalytic cycle for C–H (hetero)arene trifluoromethylation utilizing visible light. Electronic structure and photophysical studies, including TDDFT calculations, suggest Co–CF<sub>3</sub> bond homolysis at **II** occurs via an LMCT (OCO<sup>0</sup>)Co<sup>II</sup>(CF<sub>3</sub>) state, revealing ligand redox activity as a critical design feature and establishing design principles for the use of base metal chromophores for selectivity in photoredox bond activations occurring via free radical intermediates.

### TOC Graphic:



**Keywords:** trifluoromethylation, photocatalysis, redox-active ligand, base metal, cobalt

### Introduction:

The capacity of the trifluoromethyl (CF<sub>3</sub>) group to confer enhanced metabolic stability, bioavailability, lipophilicity, and potency to organic small molecules drives continued efforts to develop new methods for the selective incorporation of C–CF<sub>3</sub> bonds in pharmaceuticals and agrochemicals.<sup>1-6</sup> Methods to prepare CF<sub>3</sub>-containing molecules are versatile and robust, and include nucleophilic,<sup>7-8</sup> electrophilic,<sup>9-10</sup> and radical<sup>11</sup> CF<sub>3</sub> transfer processes. A recent emphasis on direct C–H trifluoromethylation has prompted

a revisitation of radical alkylations, which can install the CF<sub>3</sub> functional group in unactivated arenes and heteroarenes.<sup>11-12</sup> Minisci-type radical functionalization of heteroarenes is not new,<sup>13</sup> but the past decade has seen a "renaissance" in redox methods for catalytic C–H trifluoromethylation, which include the development of photoredox methods for generation of free •CF<sub>3</sub>.<sup>12, 14-19</sup> The •CF<sub>3</sub> radical is a strong electrophile, so regioselectivity in these systems, or lack thereof, is determined by the stereoelectronics of the substrate.

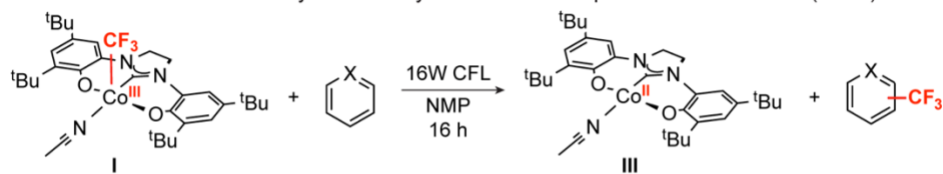
Recent advances in selective C–H functionalization by organometallic catalysts suggest a path to selectivity in C–H fluoroalkylations. However, most state-of-the-art methods for C–C coupling cannot reliably be extended to C–CF<sub>3</sub> bond formation due to intrinsic properties of the M–CF<sub>3</sub> intermediates. Whereas early transition metal M–CF<sub>3</sub> bonds readily undergo α-fluoride abstraction to generate difluoromethyl carbene complexes,<sup>20-22</sup> M–CF<sub>3</sub> bonds to low-valent later 3d metals are often thermodynamically robust and kinetically inert.<sup>23</sup> Accordingly, recent successes in the development of metal-mediated trifluoromethylations activate M–CF<sub>3</sub> bonds via formation of, for instance, high formal oxidation state complexes, which are prone to C–CF<sub>3</sub> reductive elimination.<sup>24-26</sup> In this context, photoredox activation of organometallic catalysts, termed multimetallic or metallaphotoredox catalysis,<sup>19, 27</sup> has received considerable attention for C–C bond formation, including radical alkylations from homolysis of Co(III)–alkyl complexes.<sup>28</sup> With few exceptions, these processes separate the light-harvesting species from the transition metal catalyst. The role of the chromophore—most commonly a polypyridyl Ru or Ir complex—is to directly activate the metal complex via excited state oxidation or reduction or to generate a nonmetal free radical coupling partner, which is subsequently trapped at

a transition metal center in a catalytic cycle for C–C or C–X coupling.<sup>19</sup> Although the benefits of these approaches are many, including the capacity to utilize nontraditional reaction partners in cross coupling, bimetallic excited state reactivity limits the use of base metals in photoredox catalysis.<sup>29-33</sup> Moreover, separating the chromophore from the bond-forming reaction adds a layer of complexity when pursuing metal-mediated selectivity and opens paths to side reactions from transient free radicals.

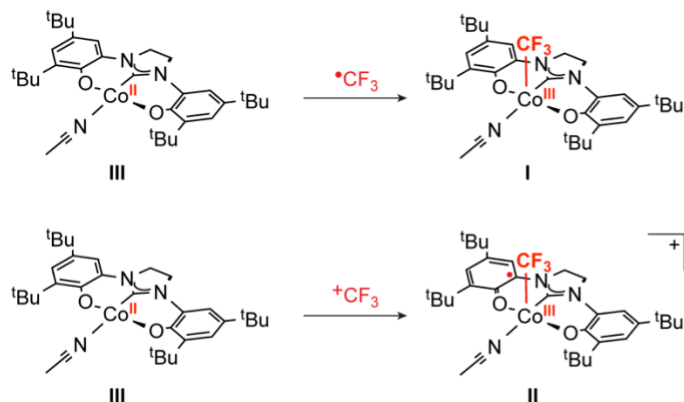
Photoinduced M–L bond activations are a staple of organometallic synthesis, and the capacity of cobaloxime organocobalt(III) complexes to generate alkyl radicals via facile Co–C homolysis has been known and exploited for synthesis applications for decades.<sup>28</sup> Such "visible light induced homolysis" (VLIH) has been proposed as a generalizable alternative to utilize 3d transition metals in photocatalytic applications.<sup>34</sup>

We reported a [(OCO)Co<sup>III</sup>(CF<sub>3</sub>)(MeCN)] (I) compound supported by a pincer-type [OCO] ligand, which trifluoromethylates unactivated (hetero)arenes upon irradiation by a broad-spectrum compact fluorescent light (CFL) (Figure 1a).<sup>35</sup> The redox-active [OCO] is an essential feature of the observed reactivity.<sup>36</sup> It provides access to a low energy LMCT [(OCO•)Co<sup>II</sup>(CF<sub>3</sub>)(MeCN)] redox isomer, which populates a Co–CF<sub>3</sub> σ\* MO, reducing the Co–C bond order to 0.5 and facilitating release of a persistent •CF<sub>3</sub> radical, which attacks electron rich arenes. The [(OCO)Co<sup>II</sup>(MeCN)] byproduct subsequently oxidizes the resulting cyclohexadienyl intermediate to afford the products of arene C–H trifluoromethylation without a sacrificial or substrate-derived oxidant. Extensions to catalysis were challenged by deactivation of the (OCO)Co<sup>III</sup>(CF<sub>3</sub>) core upon binding a sixth ligand, precluding the use of donor solvents, and competitive degradation of the silver salts used to install the CF<sub>3</sub> functionality in light.

**a. Prior work.** Stoichiometric trifluoromethylation of aryl C–H bonds via photoactivation of an (OCO)Co<sup>III</sup>–CF<sub>3</sub> bond.



**b. Co products of oxidation by different CF<sub>3</sub> reagents.**



**c. This work.** Photocatalytic C–H trifluoromethylation.

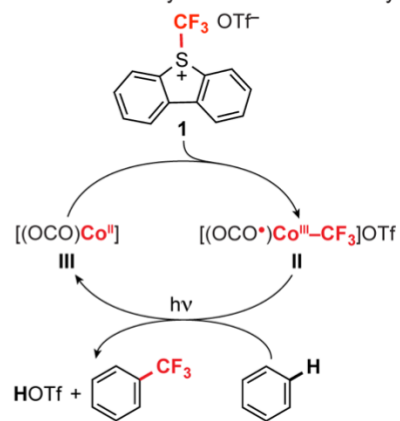


**Figure 1.** (a) Stoichiometric trifluoromethylation of heteroarene C–H bonds by photoinduced Co<sup>III</sup>–CF<sub>3</sub> bond activation.<sup>35</sup> (b) Comparison of oxidation products of Co(II) oxidation produced by formal addition of  $\bullet\text{CF}_3$  vs.  $^+\text{CF}_3$ . (c) Proposed (OCO)Co<sup>II</sup>/(OCO $\bullet$ )Co<sup>III</sup>(CF<sub>3</sub>) catalysis cycle for trifluoromethylation of benzene utilizing a  $^+\text{CF}_3$  reagent and visible light activation of **II**.

Our search for alternative sources of CF<sub>3</sub> led to electrophilic CF<sub>3</sub> reagents, such as Umemoto's S-(trifluoromethyl)dibenzothiophenium triflate (**1**), which have been extensively studied for trifluoromethylation.<sup>9, 37-40</sup> Their shelf stability and ease of handling have made them oftentimes preferred over cheaper, alternative CF<sub>3</sub> sources such as ICF<sub>3</sub> and HCF<sub>3</sub>,<sup>41</sup> and over the past decade these reagents have seen extensive use in catalytic trifluoromethylations. In reactions with these reagents, the transition metal typically acts as an outer-sphere, one-electron reductant, thus generating  $\bullet\text{CF}_3$  without M–CF<sub>3</sub> intermediates.<sup>4, 42-43</sup> Addition of a  $^+\text{CF}_3$  equivalent to a transition metal is a formal 2e<sup>−</sup> oxidation of the metal center, which demands a 2e<sup>−</sup> redox capacity at the metal center. This is exemplified by work of Sanford and coworkers, wherein formal  $^+\text{CF}_3$  transfer

generates a  $\text{Ni}^{\text{IV}}\text{-CF}_3$  complex, which is active for trifluoromethylation of unactivated arenes.<sup>44</sup>

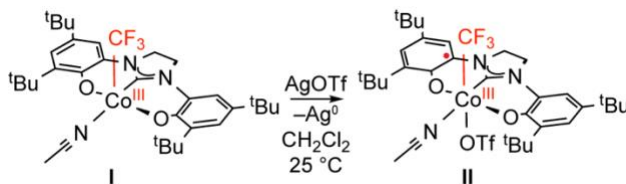
By analogy, addition of  $^+\text{CF}_3$  to our  $(\text{OCO})\text{Co}^{\text{II}}$  complex affords an  $(\text{OCO})\text{Co}(\text{CF}_3)$  species two redox levels above  $\text{Co}(\text{II})$ , and one above the  $(\text{OCO})\text{Co}^{\text{III}}(\text{CF}_3)$  that was previously demonstrated to be photoactive for trifluoromethylation (Figure 1b). Given the propensity of the redox-active  $[\text{OCO}]$  ligand to support Co in four formal oxidation states,<sup>36</sup> we speculated that net  $^+\text{CF}_3$  addition to an  $(\text{OCO})\text{Co}^{\text{II}}$  species would afford an  $(\text{OCO}^\bullet)\text{Co}^{\text{III}}(\text{CF}_3)$  product and opening avenues for catalysis based on a  $2e^-$  redox cycle (Figure 1c). But it was unclear whether  $(\text{OCO}^\bullet)\text{Co}^{\text{III}}(\text{CF}_3)$  would retain the features necessary for photoactivation of the  $\text{Co}\text{-CF}_3$  bond.

Reported herein is a Co catalyzed photoredox method for efficient trifluoromethylation of unactivated arene and heteroarene C–H bonds using **1** and visible light. Mechanistic studies and stoichiometric reactions provide strong evidence for a  $2e^-$  redox cycle involving net  $^+\text{CF}_3$  addition to a  $\text{Co}(\text{II})$  complex to generate a photoactive  $(\text{OCO}^\bullet)\text{Co}^{\text{III}}(\text{CF}_3)$  species. Combining the chromophore and organometallic reaction center in  $(\text{OCO}^\bullet)\text{Co}^{\text{III}}(\text{CF}_3)$  establishes key design principles for selectivity in photoredox radical C–H (fluoro)alkylations.

## Results:

**Preparation and electronic structure of  $[(\text{OCO})\text{Co}(\text{CF}_3)(\text{THF})\text{OTf}]$  (**II**).** Treating a burgundy  $\text{CH}_2\text{Cl}_2$  solution of  $[(\text{OCO})\text{Co}^{\text{III}}(\text{CF}_3)(\text{MeCN})_n]$  (**I**) ( $n = 1, 2$ ;  $[\text{OCO}] = 1, 3$ -bis(3,5-di-tert-butyl-2-hydroxyphenyl)imidazoline) with 1 equiv  $\text{AgOTf}$  gave an immediate color change to olive-green, from which **II** was isolated in 80% yield (Eq 1). A sample of the

THF adduct of **II** suitable for analysis by X-ray diffraction was prepared by slow evaporation of a concentrated THF:HMDSO (1:1) solution at 25 °C. The structure of **II** is shown in Figure 2a. The Co center is six-coordinate with the [OCO] pincer ligand occupying three *meridional* sites. An equatorial THF ligand is *trans* to the pincer carbene, and *trans* disposed CF<sub>3</sub> and OTf ligands complete the quasi-octahedral coordination sphere. Oxidation of **I** to **II** occurs with minor contractions (ca. 0.02 Å) of the Co–O bonds to the phenoxides and the Co–C bond to the carbene (from 1.8428(13) Å in **I** to 1.8300(10) Å in **II**). The Co–CF<sub>3</sub> bond length is statistically indistinguishable from **I** (1.914(2) Å in **II** vs. 1.918(1) Å in **I**). The [OCO] ligand bond metrics for **II** are collected in Figure 2b. As compared to **I**, the ligand metrical data shows a pronounced quinoid-type pattern of four elongated and two contracted C–C bonds in both phenoxides along with contracted C–O and C–N bonds. These changes are consistent with those expected upon ligand oxidation. Moreover, the [OCO] ligand bond lengths in **II** are nearly identical to the arithmetic mean of those in isolated complexes containing the ligand in its fully reduced [OCO]<sup>2-</sup> and doubly oxidized charge neutral [OCO]<sup>0</sup> oxidation states (Figure 2c).<sup>36</sup> In sum, the X-ray data are entirely consistent with formulation of the [OCO] ligand in **II** as a monoanionic [OCO•]<sup>-</sup> free radical with the charge distributed symmetrically across the ligand framework. Accordingly, the sum of the solid state data suggest **II** is best formulated as [(OCO•)Co<sup>III</sup>(CF<sub>3</sub>)(THF)OTf].



**Eq 1.**

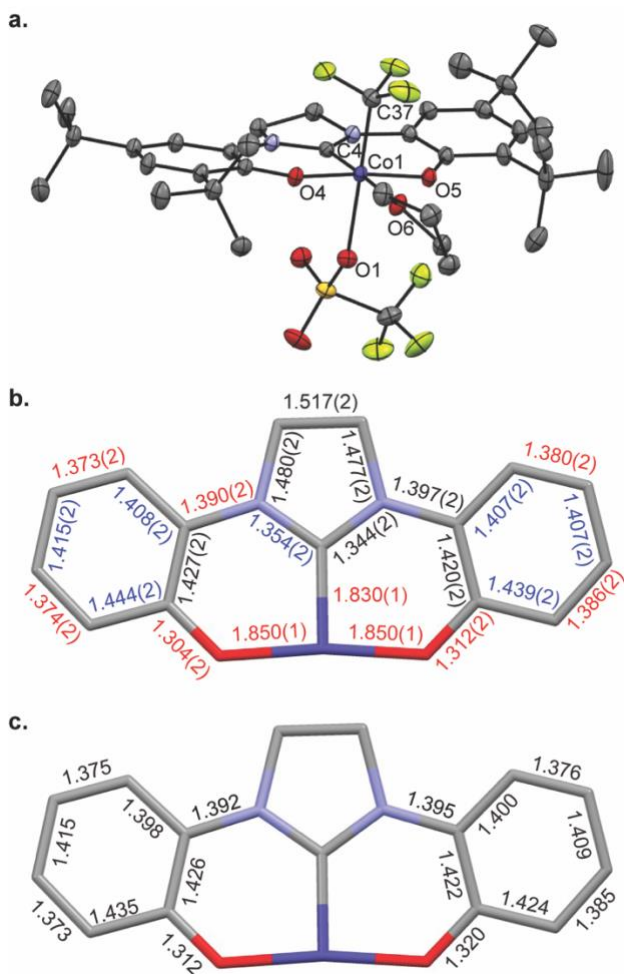


**Figure 2.** (a) ORTEP plot of  $[(\text{OCO}\cdot)\text{Co}^{\text{III}}(\text{THF})(\text{CF}_3)\text{OTf}]$  (II). Ellipsoids are drawn at 50% probability. Hydrogen atoms and non-coordinated solvent molecules are omitted for clarity. (b) Schematic of selected bond lengths (Å) for II. Bond length changes greater than 0.01 Å vs  $[(\text{OCO})\text{Co}^{\text{III}}(\text{CF}_3)(\text{MeCN})_2]$  (I) are indicated by colored labels: red indicates bond contraction; blue indicates bond elongation. (c) Arithmetic mean of the fully reduced  $[\text{OCO}]^{2-}$  ligand and the doubly oxidized charge neutral  $[\text{OCO}]^0$  form in  $[(\text{OCO})\text{Co}^{\text{II}}(\text{THF})_3]^{2+}$ .<sup>36</sup> Metrical data for the isolated  $[\text{OCO}]^{2-}$  and  $[\text{OCO}]^0$  ligands are reproduced in Figure S30.

Consistent with this assignment, the solution magnetic moment ( $\mu_{\text{eff}}$ ) of II of 1.92 in THF- $d_8$  is slightly higher than the spin-only values for an  $S = 1/2$  complex. Plausible electronic structures include a low-spin Co(III) center with a single unpaired electron on the  $[\text{OCO}\cdot]^-$  ligand or an intermediate spin  $S = 1$  Co(III) center antiferromagnetically

coupled to an  $[\text{OCO}\cdot]^-$  ligand radical. An alternative Co(II) formation with a doubly oxidized  $[\text{OCO}]^0$  ligand is inconsistent with the X-ray metrical data and the thermal stability of the Co–CF<sub>3</sub> bond (*vide infra*).

To distinguish these possibilities, the electronic structure of **II** was computed with unrestricted DFT calculations (BP86, def2-TZVP) starting in the experimentally determined doublet state. The bond lengths of the optimized geometry in the doublet state were compared to the single-crystal X-ray structure and found to have a mean absolute error of 0.013 Å. In the (OCO)Co<sup>III</sup>(CF<sub>3</sub>) fragment, a maximum bond length deviation of 0.006 Å was observed, suggesting that the spin state, functional, and basis set (BP86, def2-TZVP) used for geometry optimization accurately capture the bond distances in the complex. The spin density per atom in optimized geometry was also calculated. Complex **II** converged as a doublet ( $\langle s^2 \rangle = 0.7533$ ), with 22.4% of the total spin density being located at cobalt (Figure 3). The balance of the spin density is delocalized over both phenoxide arms of the OCO ligand, mainly on the oxygen atoms (total of 26.4%). A small amount of spin-down density on the NHC and two aryl carbons can be attributed to spin polarization. A quartet state ( $\langle s^2 \rangle = 3.7996$ ) is computed to be +33 kcal mol<sup>-1</sup> higher in energy than the doublet state, making its involvement highly unlikely. UCO analysis of  $\alpha$  and  $\beta$  orbitals showed only one orbital with an overlap integral less than 0.999: the singly occupied molecular orbital distributed across the Co center and the [OCO] ligand.<sup>45-46</sup> The computed structure of **II** is therefore most consistent with an  $[(\text{OCO}\cdot)\text{Co}^{\text{III}}(\text{CF}_3)(\text{THF})\text{OTf}]$  assignment, with a low-spin Co(III) center and a monooxidized  $[\text{OCO}\cdot]^-$  ligand radical, corroborating experimental observations and computation of very similar systems.<sup>35-36</sup> Partial delocalization of the unpaired spin onto the Co center reflects significant covalency

in the metal–ligand bonding or minor contributors to the ground state, which would not be readily evident in common spectroscopic methods.

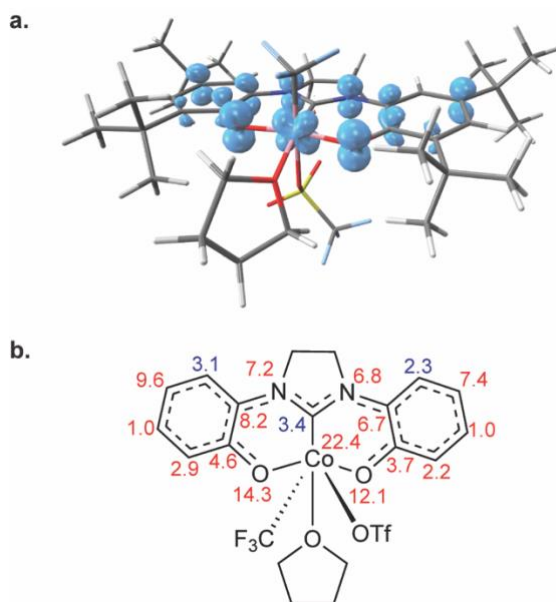


**Figure 3.** (a) Spin density plot of **II** ( $S = 1/2$ ), generated with IQMol (isosurface value 0.004). (b) Spin density per atom for **II**. Spin down density is shown in blue.

### Absorption spectrum and photochemistry of $[(\text{OCO}\cdot)\text{Co}^{\text{III}}(\text{CF}_3)(\text{THF})\text{OTf}]$ (**II**).

The UV–vis spectrum of **II** in  $\text{CH}_2\text{Cl}_2$  (Figure 4a) exhibits four CT bands at 438, 460, 518, and 889 nm ( $\epsilon = 2400\text{--}6600 \text{ M}^{-1} \text{ cm}^{-1}$ ). Excited states were examined by TDDFT calculations (BP86, def2-TZVP) from the doublet ground state. The calculated and experimental UV–vis spectra of complex **II** are in strong agreement (Figure 5a). The difference density CEJ plot of the transition at 447 nm (Figure 5b) shows strong ligand-to-metal-charge-transfer (LMCT) character and results in 89% population of the calculated LUMO (Figure 5b), which has significant antibonding character between the Co center and the  $\text{CF}_3$  ligand, suggesting photoexcitation of **II** with 447 nm light should significantly destabilize the Co– $\text{CF}_3$  bond towards homolysis.

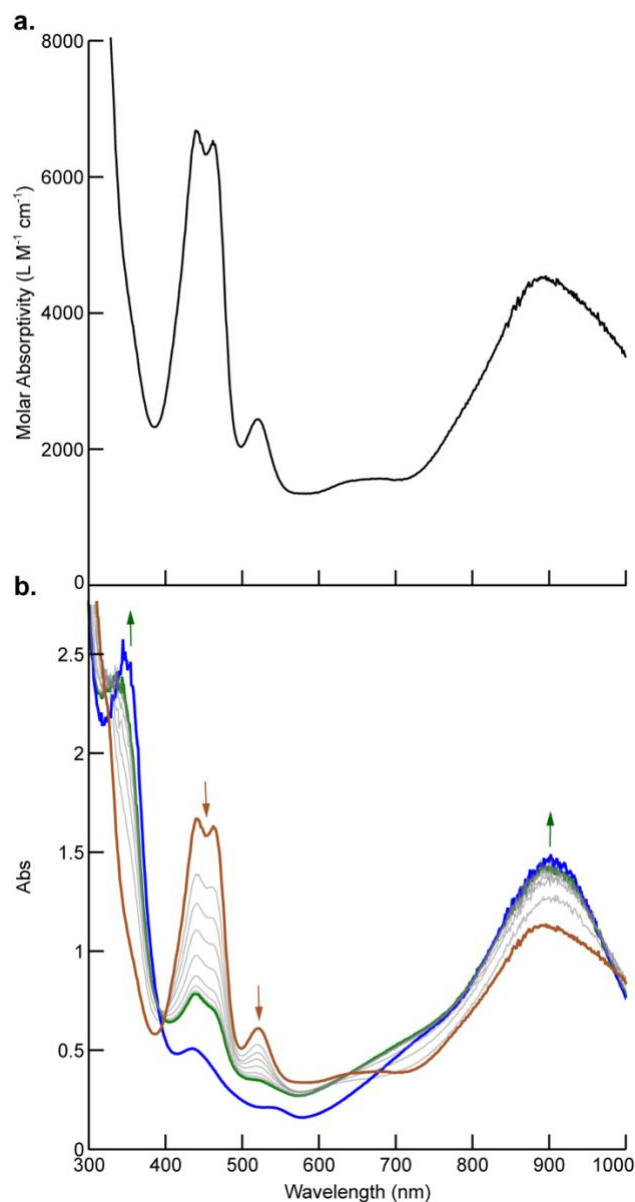


**Figure 4.** UV–vis absorption spectra of (a) 0.25 mmol **II** in CH<sub>2</sub>Cl<sub>2</sub> at 25 °C and (b) upon exposure to a Kessil® KSPR 160L-440 LED lamp. Spectra are shown at t = 0 (brown line) and 0.5 h intervals to t = 4 h (green line). A spectrum of isolated [(OCO)Co<sup>III</sup>(THF)<sub>2</sub>]OTf (**IV**) in CH<sub>2</sub>Cl<sub>2</sub> (blue line) is shown for comparison.

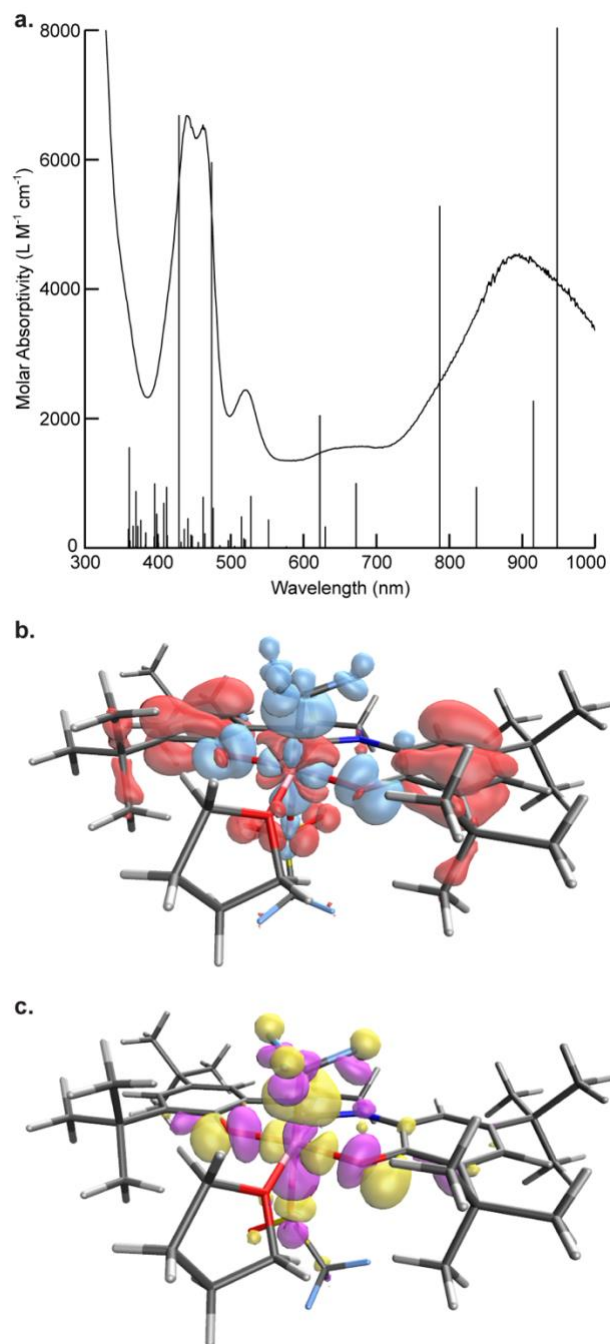


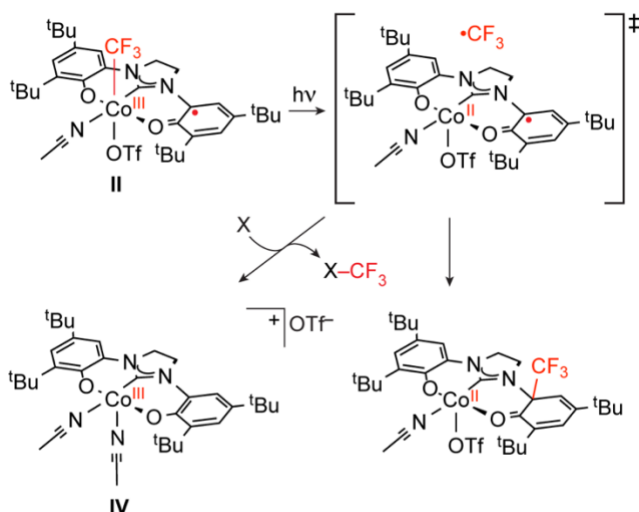
**Figure 5.** (a) Overlay of simulated and experimental UV–vis absorption spectra of **II**. (b) Difference density CEJ plot of the calculated transition at 447 nm plotted in IQMol, isovalue 0.001. Positive density is shown in blue and negative density is shown in red. (c) Calculated LUMO plotted in IQMol, isovalue 0.030.

Consistent with this hypothesis, photolysis of a 0.25 mmol solution of **II** in  $\text{CH}_2\text{Cl}_2$  using a Kessil® KSPR 160L-440 LED lamp resulted in a measurable decrease in the

intensity of the CT bands at 438, 460, and 518 nm within minutes, with a concomitant increase in intensity and a red shifting of the band at 890 nm to 902 nm and appearance of a new band at 337 nm (Figure 4b). Isosbestic points at 400 and 625 nm are consistent with clean conversion to a single product or mixture of products without formation of observable intermediates. The spectrum after 4 h of continuous photolysis closely matched that of isolated  $[(\text{OCO})\text{Co}^{\text{III}}(\text{THF})_2]\text{OTf}$  (**IV**).<sup>36</sup> Photoinduced homolysis of the  $\text{Co}^{\text{II}}-\text{CF}_3$  bond occurs at an LMCT excited state of **II** to afford an excited state intravalence isomer of **IV**. The net conversion of **II** to **IV** is balanced by loss of  $\bullet\text{CF}_3$ . The fate of the  $\bullet\text{CF}_3$  under these conditions was not determined, but  $\text{CF}_3\text{Cl}$  is most likely from reaction with  $\text{CH}_2\text{Cl}_2$  solvent. The UV-vis spectrum of **II** in  $\text{CH}_2\text{Cl}_2$  was unchanged over 7 h in the dark at 50 °C, suggesting  $\text{Co}-\text{CF}_3$  homolysis occurs from a photoexcited state and not thermolysis from heating by the light source (Figure S2).

**Photoinduced  $\bullet\text{CF}_3$  transfer from  $[(\text{OCO}\bullet)\text{Co}^{\text{III}}(\text{CF}_3)(\text{THF})\text{OTf}]$  (**II**).** Exposure of a 7.5 mM  $\text{CH}_2\text{Cl}_2$  solution of **II** containing 10 equiv 2,2,6,6-tetramethylpiperidine-1-oxyl ( $\text{TEMPO}\bullet$ ) to a 16W compact fluorescent lamp (CFL) afforded  $\text{TEMPO}-\text{CF}_3$  in 12% yield after 16 h, as determined by  $^{19}\text{F}$  NMR spectroscopy, along with unidentified  $\text{CF}_3$ -containing byproducts. Analysis of the reaction mixture by GC-MS revealed a second product with a molecular weight of 579 m/z, consistent with  $\text{CF}_3$  addition to the  $[\text{OCO}]$  ligand and demetallation. Whereas increasing the concentration of  $\text{TEMPO}\bullet$  to 15 equiv at the same concentration of **II** resulted in an increase in yield of  $\text{TEMPO}-\text{CF}_3$  to 24%, increasing both the  $\text{TEMPO}\bullet$  and **II** concentration by 60% resulted in a 40% decrease in  $\text{TEMPO}-\text{CF}_3$  yield (7%). These observations are consistent with a bifurcated reaction, wherein generation of free  $\bullet\text{CF}_3$  gives access to two competing reactions (Scheme 1).

Accordingly, increasing the TEMPO• concentration relative to **[II]** increases the probability of •CF<sub>3</sub> trapping by TEMPO• and TEMPO–CF<sub>3</sub> formation; increased [Co] increases the probability of unproductive trapping at the ligand backbone and deactivation of the complex.



**Scheme 1.** Reaction pathways for trifluoromethylation following photolysis of **II**. X = TEMPO• or (hetero)arene.

Photolysis of a 0.025 mM CH<sub>2</sub>Cl<sub>2</sub> solution of **II** using a Kessil® KSPR 160L-440 LED lamp in the presence of 5 equiv C<sub>6</sub>H<sub>6</sub> afforded α,α,α-trifluorotoluene in 10% yield after 6 h, as determined by <sup>19</sup>F NMR spectroscopy. Consistent with the partitioning experiments described above, performing the reaction in neat C<sub>6</sub>H<sub>6</sub> increased the yield of α,α,α-trifluorotoluene to 58% in 6 h. Monitoring the reaction by UV–vis spectroscopy shows the reaction occurring in two sequential phases. Consumption of **II** initially generates a spectrum that closely resembles **IV** with two quasi-isosbestic points at 637 and 405 nm (Figure 6a).<sup>36</sup> Continued photolysis results in bleaching of the intermediate peaks at 889, 732, and 443 nm with concomitant growth of a feature at 357 nm, which is diagnostic of [(OCO)Co<sup>II</sup>(THF)] (**III**) (Figure 6b). The net conversion of **II** + C<sub>6</sub>H<sub>6</sub> to **III** +

$\alpha,\alpha,\alpha$ -trifluorotoluene is balanced by loss of 1 equiv HOTf (Eq 2). HOTf formation, in the form of a triflate salt, is evident in catalytic reactions as a singlet at  $-79$  ppm in the  $^{19}\text{F}$  NMR spectrum of reactions performed in J. Young NMR tubes (*vide infra*).<sup>47</sup> Its appearance in stoichiometric reactions, however, is frequently obscured, presumably by an interaction with paramagnetic **III** or a rapid exchange process. Accordingly, addition of 1.0 equiv Hünig's *N,N*-diisopropylethylamine (*i*Pr<sub>2</sub>EtN) base to reaction mixtures of **II** + C<sub>6</sub>H<sub>6</sub> resolves the HOTf byproduct as [*i*Pr<sub>2</sub>EtNH]OTf, which is manifested in the  $^{19}\text{F}$  NMR spectrum as a sharp singlet at  $-79$  ppm upon photolysis (Figure S9-S10).

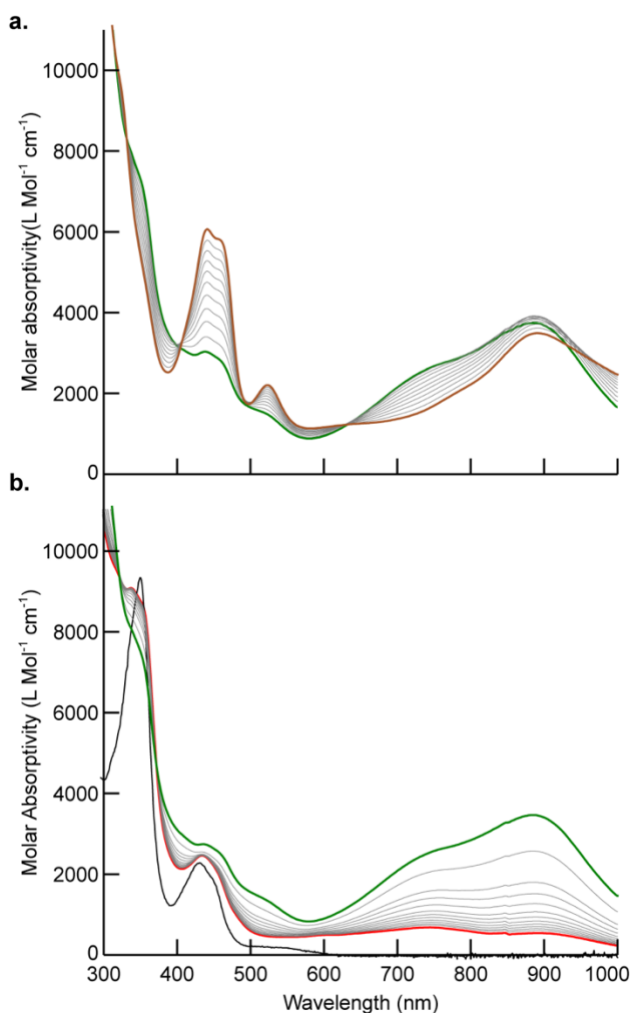
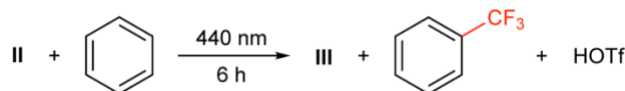


**Figure 6.** Absorption spectra of (a) 0.23 mmol **II** in C<sub>6</sub>H<sub>6</sub> with exposure to ambient light. Spectra are shown at 5 min intervals from  $t = 0$  (brown) to  $t = 55$  min (green). (b) A 0.23

mmol solution of **II** in C<sub>6</sub>H<sub>6</sub> upon exposure to ambient light. Spectra are shown from t = 55 m (green) and 5 min intervals to t = 120 m (red). A spectrum of isolated [(OCO)Co<sup>II</sup>(THF)] (**III**) in C<sub>6</sub>H<sub>6</sub> (black) is shown for comparison.



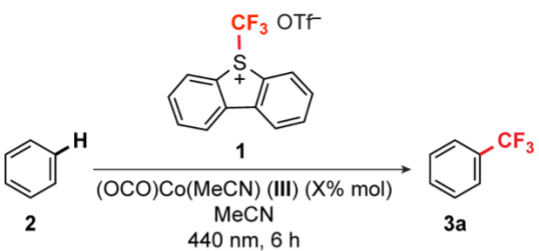
## Eq 2

**Photocatalytic arene C–H trifluoromethylation.** Addition of a <sup>+</sup>CF<sub>3</sub> fragment to the Co center in **III** affords **II** via a 2e<sup>-</sup> process analogous to oxidative addition (Figure 1b). Accordingly, reactions with Umemoto's tetrafluoro-S-(trifluoromethyl)dibenzothiophenium triflate (**1**) were pursued with the aim of closing a catalytic cycle for photocatalytic arene C–H trifluoromethylation.

A combination of **III** (5 mol%) with a 1:1 mixture of C<sub>6</sub>H<sub>6</sub> and Umemoto's S-(trifluoromethyl)dibenzothiophenium triflate (**1**) in MeCN afforded α,α,α-trifluorotoluene in 18% yield after 6 h of continuous irradiation using a 440 nm blue LED lamp. (Table 1, entry 4). Major byproducts included trifluoromethylated dibenzothiophenes, which result from attack of the promiscuous •CF<sub>3</sub> radical on the heteroarene product of <sup>+</sup>CF<sub>3</sub> removal from **1**.<sup>48</sup> Accordingly, increasing the ratio of C<sub>6</sub>H<sub>6</sub> to **1** to 5:1 gave a three-fold increase in yield of α,α,α-trifluorotoluene and significantly depressed the competitive dibenzothiophene trifluoromethylation (Table 1, entry 6). A maximum yield of α,α,α-trifluorotoluene was observed with a 10-fold excess of C<sub>6</sub>H<sub>6</sub> substrate (Table 1, entries 7 and 8). Control experiments performed without cobalt gave a maximum yield of 35% (Table 1, entries 1 and 2), but in all cases the yield of α,α,α-trifluorotoluene is significantly increased by the addition of **III**. Use of CoCl<sub>2</sub> in place of **III** gave a statistically insignificant increase in the measured yield relative to the metal-free conditions (Table 1, entry 3).

Reactions performed in the dark with and without **III** gave no measurable  $\alpha,\alpha,\alpha$ -trifluorotoluene (Table 1, entries 9 and 10).

**Table 1.** Optimization of Reaction Conditions



Entry	catalyst (mol %)	<b>2</b> (equiv vs <b>1</b> )	Yield (%) <sup>a</sup>
1	none	1	20
2	none	10	35
3	CoCl <sub>2</sub> (5)	10	42
4	<b>III</b> (5)	1	18
5	<b>III</b> (5)	3	43
6	<b>III</b> (5)	5	58
7	<b>III</b> (5)	10	73
8	<b>III</b> (5)	20	73
9 <sup>b</sup>	none	10	0
10 <sup>b</sup>	<b>III</b> (5)	10	<1
11	<b>II</b> (5)	10	74

<sup>a</sup>Yields were determined by integration of <sup>19</sup>F NMR resonances using C<sub>6</sub>F<sub>6</sub> as an internal standard based on **1** as the limiting reagent, as described in the Supporting Information.

<sup>b</sup>Reaction performed in the dark.

The scope of the C–H trifluoromethylation was evaluated using six different (hetero)arene substrates (Figure 7). There was no significant change in yield when making the arene ring more electron rich (**3b**); there was a significant decrease in yield when the ring was more electron poor (**3c**). Pyrrole (**3d**) exhibited high yield and excellent selectivity with the only isomer formed being trifluoromethylation at the 2-position of the

ring. Indole (**3e**) showed moderate reactivity, but poor selectivity with an overall 35% yield and a 1:1 ratio between the 2- and 3-positions of the indole backbone.

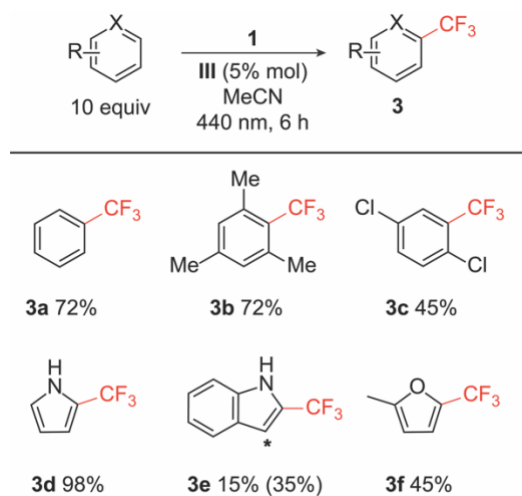
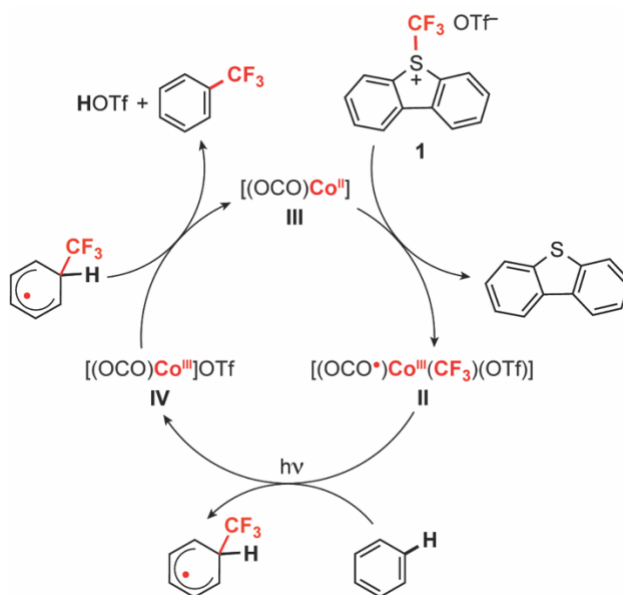


**Figure 7.** Photocatalytic trifluoromethylations of arenes and heteroarenes using **1**. Yields were determined by integration of  $^{19}\text{F}$  NMR resonances, as described in the Supporting Information. In cases where multiple isomers are formed, the overall yield is reported in parentheses.

A series of reactions were performed to probe the nature of the active catalyst. Treatment of a dark orange solution of **III** in  $\text{CH}_2\text{Cl}_2$  with 1 equiv **1** in the absence of light gave an immediate color change to dark olive-green. Monitoring the reaction by UV-vis spectroscopy showed the complete disappearance of diagnostic bands for **III** at 355 and 438 nm and the commensurate appearance of a spectrum with features at 451, 518, and 890 nm (Figure S3), which matches a 1:1 mixture of **II** and **IV**. The 50% yield of **II** in the stoichiometric reaction apparently results from photodegradation of **II** during the synthesis, suggesting the combination of **III** + **1** is a path to photoactive **II** and providing entry to functional catalysis. Accordingly, mixing **III** with 20 equiv **1** in a MeCN solution containing 200 equiv  $\text{C}_6\text{H}_6$  in the dark gave full consumption of the diagnostic CT bands for **III** and 80% conversion to **II** (Figure S4). Finally, irradiation of an acetonitrile solution

containing **II** (5 mol%), **1**, and 10 equiv C<sub>6</sub>H<sub>6</sub> with 440 nm blue LED light gave  $\alpha,\alpha,\alpha$ -trifluorotoluene in 74% yield over 6 hours (Table 1, entry 11), suggesting that **III** and **II** give entry to the same catalytic cycle, and **II** is an active intermediate for trifluoromethylation (Scheme 2).



**Scheme 2.** Experimentally demonstrated steps for photoredox trifluoromethylation of (hetero)arenes using **II** or **III** via intermediate **IV**.

### Discussion:

The capacity of (OCO)Co(CF<sub>3</sub>) complexes to generate •CF<sub>3</sub> radical upon photoexcitation is predicated on population of an MO that is primarily Co–CF<sub>3</sub>  $\sigma^*$  in nature. Accordingly, our previous successes in visible light-induced stoichiometric arene C–H trifluoromethylations using **I** utilized low energy LMCT from a ligand centered HOMO on the reduced form of the redox active [OCO]<sup>2-</sup> ligand to a d<sub>z</sub><sup>2</sup>-centered LUMO to weaken the Co–CF<sub>3</sub> bond by reduction of the formal bond order to 0.5 and promote Co–CF<sub>3</sub> homolysis.<sup>35</sup> In theory, 1e<sup>-</sup> oxidation of **I** to a formal Co(IV) center in **II** should critically

perturb multiple essential elements of this delicate framework. In practice, the redox plasticity afforded by the [OCO] ligand provides a robust mechanism to retain key design features and extend the stoichiometric photochemistry to a functional  $2e^-$  photoredox catalytic cycle.

The Co cores of complexes **I** and **II** are functionally unchanged upon oxidation. As in **I**, structural and computational data suggest that **II** is best formulated as a low-spin Co(III) center, and the computed LUMO is primarily Co–CF<sub>3</sub>  $\sigma^*$  antibonding. Accordingly, the Co<sup>III</sup>–CF<sub>3</sub> bond in **II** is thermodynamically robust—it is indefinitely stable in the dark—but is photochemically activated by population of the lowest-lying unoccupied metal-centered orbital. The bias for a low-spin Co(III) center in the (OCO)Co(CF<sub>3</sub>) core drives formation of the [OCO•]<sup>-</sup> ligand oxidation state in **II**, which was not observed in previous reports of closely related electron transfer series.<sup>36</sup>

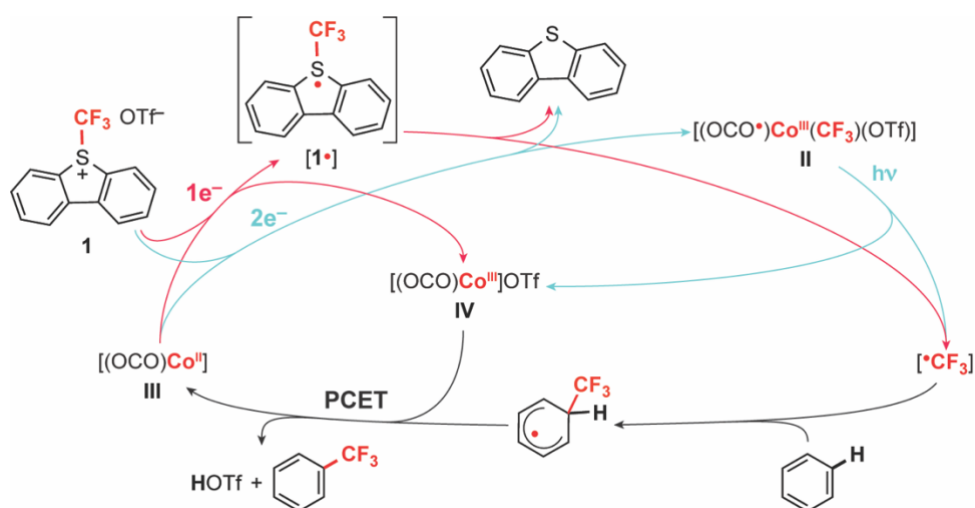
Ligand-centered oxidation impacts the photophysical properties of **II**. Both **I** and **II** feature [OCO] ligand-centered HOMOs of  $\pi$  symmetry, which are the loci of the oxidations in the photochemically active LMCT excited states. Electrostatic principles suggest that oxidation of the [OCO•]<sup>-</sup> ligand in **II** should be significantly more challenging than in the fully reduced [OCO]<sup>2-</sup> ligand in **I**. This is evident in the absorption CT band that engenders the photochemical behavior, which is shifted from 738 nm in **I** to 438 nm in **II**. This shift likely also reflects differences in the coordination environment about cobalt. Square pyramidal **I** is deactivated by binding a sixth ligand trans to CF<sub>3</sub> because the energy of the  $\sigma^*$   $d_z^2$  MO is raised above  $d_{x^2-y^2}$ .<sup>35</sup> The solid-state structure of **II** contains a <sup>-</sup>OTf ligand in the sixth site, giving **II** quasi-octahedral geometry. Simple MO arguments would expect <sup>-</sup>OTf coordination to similarly raise the energy of the photoactive  $d_z^2$  LUMO, but this is

insufficient to deactivate **II**. Computational data suggests a  $d_{z^2}$ -like orbital is still the primary contributor to the LUMO in **II**. The possibility of equilibrium  $^-OTf$  dissociation generating a photochemically active five-coordinate species cannot be ruled out under the catalysis conditions, but the fact that **II** retains its photosensitivity in MeCN solvent argues against deactivation in octahedral geometries. This makes **II** more versatile by giving access to a wider range of solvents and opening avenues for trifluoromethylation of substrates that can act as strong  $\sigma$  donors to Co, as described below.

As a stoichiometric source of free  $\bullet CF_3$  radical, **II** suffers in comparison to **I**. Under analogous conditions, the yield of  $\alpha,\alpha,\alpha$ -trifluoromethyltoluene from  $C_6H_6$  is reduced from >99% to 58%. The origin of this disparity is apparently an enhanced propensity of **II** to trap  $\bullet CF_3$  via C–C coupling to the ligand backbone, which subsequently induces demetallation and formation of unidentified Co byproducts (Scheme 1). No evidence for ligand centered  $\bullet CF_3$  radical coupling has been observed in photolysis of **I**. It is tempting to ascribe this partitioning to the presence of unpaired spin on the  $[OCO\bullet]^-$  ligand making **II** a more effective radical trap, but radical character on the arene is not a prerequisite for radical coupling and the relative kinetics of the C–C bond forming reactions in the excited states are entirely unknown at this time. This flaw is not fatal, however. Competitive trapping at the ligand can be disfavored by lowering the concentration of **II** and increasing the relative concentration of the organic acceptor. That is, the conditions one would typically pursue in catalysis are exactly those required for high-yielding reactions with the organic substrates.

Clean conversion of **III** to **II** using **1** establishes all the steps required for functional photocatalysis, as illustrated in Scheme 2. The use of **1** here demands a multielectron

redox capacity that would typically limit the use of cobalt, as the thermodynamically preferred oxidation +2 and +3 states are incompatible with the formal  $2e^-$  redox change that occurs upon  ${}^+\text{CF}_3$  addition to the metal center. The redox active [OCO] ligand sidesteps this issue by coupling  $1e^-$  redox at cobalt with  $1e^-$  oxidation at the ligand, as shown in the blue pathway in Scheme 3. The net  $2e^-$  reaction can occur without accumulation of  $1e^-$  intermediates because of strong electronic coupling and covalency in the Co–OCO bonding.<sup>36</sup>



**Scheme 3.** Proposed photocatalysis mechanisms of arene trifluoromethylation using **III**.

Given its well-established propensity to participate in radical  $\bullet\text{CF}_3$  transfer, the use of **1** as a  $\text{CF}_3$  source merits additional discussion. Although **1** was initially conceived as a source of  ${}^+\text{CF}_3$ , radical mechanisms have been frequently invoked.<sup>49</sup> These suggest initial  $1e^-$  transfer generates a reduced form of Umemoto's reagents ( $1\bullet$  in Scheme 3), which is itself a source of  $\bullet\text{CF}_3$  radical. Accordingly, single electron transfer (SET) and radical chain mechanisms have been suggested for trifluoromethylations using **1** with common photoreductants or reducing metals in their ground state.<sup>43-44, 48, 50-52</sup> Ground state initial ET, illustrated by the red  $1e^-$  path Scheme 3, is unlikely here based on the redox

potentials of the reactants. Whereas **1** is reduced at  $-0.75$  V vs  $\text{Fc}^+/\text{Fc}$ ,<sup>51-52</sup> oxidation of **III** occurs at  $-0.32$  V vs  $\text{Fc}^+/\text{Fc}$ ,<sup>36</sup> implying initial outer-sphere  $1e^-$  transfer is uphill by over 400 mV. Moreover, reaction of **III** with **1** in the dark gives exclusively **II**; ruling out  $1^\bullet$  as a viable route to trifluoromethylated arene in the absence of light.

Direct photoactivation of **1** has been reported and suggested to occur via *in situ* generation of  $\pi-\pi$  complexes with arenes, which are competent visible light chromophores.<sup>53-54</sup> This may account for the significant background reactivity observed herein. To our knowledge, the excited state reduction potential of **1** is unknown. Accordingly, the red  $1e^-$  pathway cannot be rigorously excluded as a contributor to the observed catalysis under constant photolysis.

Irradiation of **II** with visible light induces facile  $\text{Co}-\text{CF}_3$  bond homolysis to generate a persistent  $^\bullet\text{CF}_3$  electrophile capable of attacking (hetero)arenes (Scheme 3). Re-aromatization of the initially formed cyclohexadienyl radical requires net loss of  $\text{H}^\bullet$ . Formation of **III** in these reactions implies a net  $2e^-$  reduction of the cobalt center, and UV-vis data are consistent with this occurring by two consecutive  $1e^-$  steps via the  $\text{Co(III)}$  intermediate **IV**. The role of **IV** is an outer-sphere  $1e^-$  oxidant rather than an  $\text{H}^\bullet$  acceptor. The net PCET reaction is balanced by loss of  $\text{H}^+$  in the form of HOTf, which apparently generates dibenzothiophenium triflate under the catalysis conditions.<sup>55</sup>

Throughout this manuscript, the ligand *trans* to the carbene in the [OCO] ligand is largely ignored because it is a spectator. Work on these and closely related ET series have revealed a capacity to bind a range of O- and N-donor substrates, including furans, pyridines, and nitriles in this position.<sup>35-36</sup> The photochemistry of **II** is seemingly unaffected by substitution at this site. Accordingly, the selectivity reported herein is determined by

the persistent  $\bullet\text{CF}_3$  radical and the arene substrates themselves. Trifluoromethylation of the [OCO] ligand demonstrates the capacity of an inner-sphere radical acceptor to function as a competitive trap, presumably via geminate recombination, suggesting an oriented substrate should be similarly susceptible to aryl trifluoromethylation within the solvent cage.

### **Conclusion:**

The novelty of the catalysis reported herein is not the organic products, the use of light to generate  $\bullet\text{CF}_3$  radical, or even the application of organocobalt(III) complexes for trifluoromethylation, but rather extrapolation of the catalyst design principles for photolytic C–H arene trifluoromethylation to functional catalysis and the avenues for selective photoredox catalysis that result. Redox noninnocence of the [OCO] ligand is a central and essential feature of every step of the catalysis cycle. First, by imparting a multielectron redox capacity at Co, it permits use of  $\text{CF}_3$  sources that demand formal  $2e^-$  oxidation of the metal center to generate the active organometallic intermediate while circumventing high energy Co(IV) or Co(I) species. Second, the ligand redox flexibility preserves the low spin  $\text{Co}^{\text{III}}\text{--CF}_3$  core across multiple formal oxidations states, which makes the complexes thermodynamically inert but photochemically labile. Finally, the capacity of the [OCO] framework to be oxidized at modest potentials provides a reservoir of accessible ligand-centered electrons for generation of the photochemically active LMCT state with low energy light. The result is a coordination complex that functions as a combined chromophore and organometallic reaction center for a visible light photoredox catalysis cycle, obviating the requirement for long excited-state lifetimes which often limit the use

of base metals in photoredox catalysis. The VLIH design principles elaborated in this system are broadly transferrable; our ongoing work is focused on extensions to other, inexpensive sources of  $\text{CF}_3$ , structural modifications to tune the absorption properties and photochemistry of the organometallic chromophores, and selectivity in radical C–H trifluoroalkylations of heteroarenes that derives from spatial proximity of the C–H bonds to the incipient  $\bullet\text{CF}_3$  rather than the substrate electronics.

## **Experimental:**

### *General Considerations.*

Unless otherwise mentioned, all operations were carried out under anaerobic conditions using standard vacuum line techniques or in an inert-atmosphere glovebox under nitrogen. All NMR spectra were recorded on a Varian Mercury 400 spectrometer and chemical shifts are reported in parts per million (ppm) relative to TMS, with the residual solvent peak as an internal reference.<sup>56</sup> All  $^{19}\text{F}$  chemical shifts are reported in ppm relative to  $\text{CFCl}_3$  with hexafluorobenzene as an internal standard. Solution magnetic moments were obtained by the Evan's NMR method.<sup>57-58</sup> UV–vis absorption spectra were acquired using a Hitachi 4150 spectrophotometer. Unless otherwise noted, all electronic absorption spectra were recorded at ambient temperature in a 1 cm quartz cell. All mass spectra were recorded in the Georgia Institute of Technology Bioanalytical Mass Spectrometry Facility. Electrospray Ionization mass spectrometry (ESI-MS) was carried out with acetonitrile solutions using a Micromass Quattro LC spectrometer. Elemental analyses were performed by Atlantic Microlab, Inc., Norcross, GA. All analyses were performed in

duplicate, and the reported compositions are the average of the two runs. Full details of X-ray data collection and refinement are provided in the Supporting information.

*Materials and methods:*

Anhydrous acetonitrile (MeCN), dichloromethane (CH<sub>2</sub>Cl<sub>2</sub>), benzene, tetrahydrofuran (THF), pentane, and toluene solvents for air- and moisture-sensitive manipulations were purchased from Sigma-Aldrich and further dried by passage through columns of activated alumina, degassed by at least three freeze-pump-thaw cycles, and stored under N<sub>2</sub> prior to use. Hexamethyldisiloxane (HMDSO) was degassed by at least three freeze-pump-thaw cycles and stored over activated 4 Å molecular sieves under N<sub>2</sub> prior to use. Methanol (Drisolv) was purchased from EMD Millipore and used as received. Deuterated solvents were purchased from Cambridge Isotope Laboratories. Acetonitrile-*d*<sub>3</sub>, DCM-*d*<sub>2</sub>, and THF-*d*<sub>8</sub> were placed in an oven dried sealable flask and degassed by freeze-pump-thaw cycles then stored over activated 4 Å molecular sieves under N<sub>2</sub> prior to use. AgCF<sub>3</sub> was prepared according to a published procedure.<sup>59</sup> Silver fluoride (Strem), TMSCF<sub>3</sub> (Oakwood), Umemoto's reagent (Sigma), hexafluorobenzene (Sigma) were all used as received. [(OCO)Co(THF)],<sup>36</sup> [(OCO)Co(THF)<sub>2</sub>]OTf (**IV**),<sup>36</sup> and [(OCO)Co(CF<sub>3</sub>)(MeCN)] (**I**)<sup>35</sup> were prepared by published procedures.

**Synthesis of [(OCO)CoCF<sub>3</sub>(THF)OTf] (**II**).** A 20 mL scintillation vial was charged with [(OCO)Co(CF<sub>3</sub>)(MeCN)] (**I**) (150 mg, 0.232 mmol) in DCM (5 mL). To this solution, a suspension of AgOTf (63 mg, 0.25 mmol) in DCM (2 mL) was added dropwise and an immediate color change from burgundy red to dark green occurred. After stirring for 3 hours, the reaction as was filtered through a 2mm pad of Celite and washed with DCM until the washings were no longer colored. The filtrate was concentrated *in vacuo*

affording a dark olive-green colored solid **II** (180 mg, 0.226 mmol, 98%). X-ray suitable crystals were grown from a concentrated 1:1 (THF:HMDSO) solution that was evaporated over 2 days resulting in dark-green plates. Satisfactory elemental analysis required the inclusion of one H<sub>2</sub>O, which has been observed in structures obtained from wet solvents; the reported analysis is for [(OCO)Co(CF<sub>3</sub>)(MeCN)(OH<sub>2</sub>)]OTf. Anal. Calc. for C<sub>35</sub>H<sub>49</sub>CoF<sub>6</sub>N<sub>3</sub>O<sub>6</sub>S: C, 51.72; H, 6.08; N, 5.17; Found: C, 52.10; H, 6.22; N, 4.82. HR-ESI-MS (*m/z*): 604.2663 [M-THF-OTf]<sup>+</sup>. UV-vis (DCM) λ<sub>max</sub>, nm (ε, M<sup>-1</sup>cm<sup>-1</sup>): 442 (6672), 461 (6475), 523 (2411), 895 (4550).

### **C–H Trifluoromethylation of (Hetero)Aryls.**

In a representative procedure, a borosilicate NMR tube with a J Young valve was charged with **1** (80.5 mg, 0.2 mmol), C<sub>6</sub>H<sub>6</sub> (180 μL, 2 mmol, 10 equiv.), **III** (5 mg, .01 mmol, 5% mol) and CD<sub>3</sub>CN (1 mL). The tube was sealed and placed ~3 inches from a Kessil® KSPR 160L-440 LED lamp for 6 hours. Hexafluorobenzene (11.5 μL, 0.1 mmol) was added as an internal standard and yields were measured by integration against the <sup>19</sup>F resonances for the CF<sub>3</sub> containing products. The NMR spectra matched those previously reported.<sup>14</sup>

44, 50, 60-62

### **Computational Studies.**

DFT calculations were performed using ORCA 4.2.1<sup>63-64</sup> using the BP86<sup>65-66</sup> functional and def2-TZVP<sup>67-68</sup> basis set (default grid) on the full model. TD-DFT calculations were performed at the same level of theory using the output coordinates from the geometry optimization as input. Spin density, difference density, and molecular orbital plots were generated using IQmol (<http://www.iqmol.org/>), and IboView (<http://www.iboview.org/>).

## Supporting Information.

Details of photolysis apparatus; UV–vis absorption data for thermal stability study of **II** and selected reactions of **III** with **1**;  $^{19}\text{F}$  NMR spectra for stoichiometric photolysis reactions of **II** and catalytic reactions with **1** and/or **III** and substrates; ESI–MS data for **II** and a photolysis reaction of **II** with TEMPO $^{\bullet}$ ; selected X-ray crystallographic data for **II**, **III**, and  $[(\text{OCO}^0)\text{Co}^{\text{II}}(\text{THF})_3](\text{PF}_6)_2$ ; complete X-ray structure report for **II**; DFT Orca input files and TDDFT orbitals and transition states for **II**.

## Acknowledgements:

We gratefully acknowledge the National Science Foundation (grant number CHE 2102292 to JDS) for financial support of this work. We thank David Bostwick for mass spectrometry assistance. The DFT and TDDFT sections of this work were supported through research cyberinfrastructure resources and services provided by the Partnership for an Advanced Computing Environment (PACE) at the Georgia Institute of Technology.

## References:

1. Hagmann, W. K., The many roles for fluorine in medicinal chemistry. *J. Med. Chem.* **2008**, *51*, 4359-4369.
2. Purser, S.; Moore, P. R.; Swallow, S.; Gouverneur, V., Fluorine in medicinal chemistry. *Chem. Soc. Rev.* **2008**, *37*, 320-330.
3. Jeschke, P., The unique role of halogen substituents in the design of modern agrochemicals. *Pest Management Science* **2010**, *66*, 10-27.
4. Wang, J.; Sanchez-Rosello, M.; Acena, J. L.; del Pozo, C.; Sorochinsky, A. E.; Fustero, S.; Soloshonok, V. A.; Liu, H., Fluorine in Pharmaceutical Industry: Fluorine-Containing Drugs Introduced to the Market in the Last Decade (2001-2011). *Chem. Rev.* **2014**, *114*, 2432-2506.

5. Meanwell, N. A., Fluorine and Fluorinated Motifs in the Design and Application of Bioisosteres for Drug Design. *J. Med. Chem.* **2018**, *61*, 5822-5880.
6. Intermaggio, N. E.; Millet, A.; Davis, D. L.; MacMillan, D. W. C., Deoxytrifluoromethylation of Alcohols. *J. Am. Chem. Soc.* **2022**, *144*, 11961-11968.
7. Prakash, G. K. S.; Yudin, A. K., Perfluoroalkylation with organosilicon reagents. *Chem. Rev.* **1997**, *97*, 757-786.
8. Liu, X.; Xu, C.; Wang, M.; Liu, Q., Trifluoromethyltrimethylsilane: Nucleophilic Trifluoromethylation and Beyond. *Chem. Rev.* **2015**, *115*, 683-730.
9. Umemoto, T., Electrophilic perfluoroalkylating agents. *Chem. Rev.* **1996**, *96*, 1757-1777.
10. Charpentier, J.; Fruh, N.; Togni, A., Electrophilic Trifluoromethylation by Use of Hypervalent Iodine Reagents. *Chem. Rev.* **2015**, *115*, 650-682.
11. Studer, A., A "Renaissance" in Radical Trifluoromethylation. *Angew. Chem. Int. Ed* **2012**, *51*, 8950-8958.
12. Gurry, M.; Aldabbagh, F., A new era for homolytic aromatic substitution: replacing Bu<sub>3</sub>SnH with efficient light-induced chain reactions. *Org. Biomol. Chem.* **2016**, *14*, 3849-62.
13. Duncton, M. A. J., Minisci reactions: Versatile CH-functionalizations for medicinal chemists. *Medchemcomm* **2011**, *2*, 1135-1161.
14. Nagib, D. A.; MacMillan, D. W. C., Trifluoromethylation of arenes and heteroarenes by means of photoredox catalysis. *Nature* **2011**, *480*, 224-228.
15. Ji, Y. N.; Brueckl, T.; Baxter, R. D.; Fujiwara, Y.; Seiple, I. B.; Su, S.; Blackmond, D. G.; Baran, P. S., Innate C-H trifluoromethylation of heterocycles. *Proc. Natl. Acad. Sci. U.S.A.* **2011**, *108*, 14411-14415.
16. Koike, T.; Akita, M., Trifluoromethylation by Visible-Light-Driven Photoredox Catalysis. *Top. Catal.* **2014**, *57*, 967-974.
17. Romero, N. A.; Nicewicz, D. A., Organic Photoredox Catalysis. *Chem. Rev.* **2016**, *116*, 10075-10166.
18. Michelin, C.; Hoffmann, N., Photosensitization and Photocatalysis—Perspectives in Organic Synthesis. *ACS Catal.* **2018**, *8*, 12046-12055.
19. Shaw, M. H.; Twilton, J.; MacMillan, D. W. C., Photoredox Catalysis in Organic Chemistry. *J. Org. Chem.* **2016**, *81*, 6898-6926.

20. Hughes, R. P., Organo-transition metal compounds containing perfluorinated ligands. In *Advances in organometallic chemistry*, Elsevier: 1990; Vol. 31, pp 183-267.
21. Huang, D. J.; Koren, P. R.; Folting, K.; Davidson, E. R.; Caulton, K. G., Facile and reversible cleavage of C-F bonds. Contrasting thermodynamic selectivity for Ru-CF<sub>2</sub>H vs F--Os=CFH. *J. Am. Chem. Soc.* **2000**, *122*, 8916-8931.
22. Huang, D.; Caulton, K. G., New Entries to and New Reactions of Fluorocarbon Ligands. *J. Am. Chem. Soc.* **1997**, *119*, 3185-3186.
23. Tomashenko, O. A.; Grushin, V. V., Aromatic Trifluoromethylation with Metal Complexes. *Chem. Rev.* **2011**, *111*, 4475-4521.
24. Bour, J. R.; Camasso, N. M.; Sanford, M. S., Oxidation of Ni(II) to Ni(IV) with Aryl Electrophiles Enables Ni-Mediated Aryl-CF<sub>3</sub> Coupling. *J. Am. Chem. Soc.* **2015**, *137*, 8034-8037.
25. Liu, L.; Xi, Z., Organocopper(III) Compounds with Well-defined Structures Undergo Reductive Elimination to Form C—C or C—Heteroatom Bonds. *Chin. J. Chem.* **2018**, *36*, 1213-1221.
26. Liu, S.; Liu, H.; Liu, S.; Lu, Z.; Lu, C.; Leng, X.; Lan, Y.; Shen, Q., C(sp<sup>3</sup>)-CF<sub>3</sub> Reductive Elimination from a Five-Coordinate Neutral Copper(III) Complex. *J. Am. Chem. Soc.* **2020**, *142*, 9785-9791.
27. Ackerman-Biegasiewicz, L. K. G.; Kariofillis, S. K.; Weix, D. J., Multimetallic-Catalyzed C—C Bond-Forming Reactions: From Serendipity to Strategy. *J. Am. Chem. Soc.* **2023**, *145*, 6596-6614.
28. Demarteau, J.; Debuigne, A.; Detrembleur, C., Organocobalt Complexes as Sources of Carbon-Centered Radicals for Organic and Polymer Chemistries. *Chem. Rev.* **2019**, *119*, 6906-6955.
29. McCusker, J. K., Electronic structure in the transition metal block and its implications for light harvesting. *Science* **2019**, *363*, 484-488.
30. Arias-Rotondo, D. M.; McCusker, J. K., The photophysics of photoredox catalysis: a roadmap for catalyst design. *Chem. Soc. Rev.* **2016**, *45*, 5803-5820.
31. Wenger, O. S., Is Iron the New Ruthenium? *Chem.–Eur. J.* **2019**, *25*, 6043-6052.
32. Larsen, C. B.; Braun, J. D.; Lozada, I. B.; Kunnus, K.; Biasin, E.; Kolodziej, C.; Burda, C.; Cordones, A. A.; Gaffney, K. J.; Herbert, D. E., Reduction of Electron Repulsion in Highly Covalent Fe-Amido Complexes Counteracts the Impact of a Weak Ligand Field on Excited-State Ordering. *J. Am. Chem. Soc.* **2021**, *143*, 20645-20656.

33. Wenger, O. S., Photoactive Complexes with Earth-Abundant Metals. *J. Am. Chem. Soc.* **2018**, *140*, 13522-13533.
34. Abderrazak, Y.; Bhattacharyya, A.; Reiser, O., Visible-Light-Induced Homolysis of Earth-Abundant Metal-Substrate Complexes: A Complementary Activation Strategy in Photoredox Catalysis. *Angew. Chem. Int. Ed* **2021**, *60*, 21100-21115.
35. Harris, C. F.; Kuehner, C. S.; Bacsa, J.; Soper, J. D., Photoinduced Cobalt(III)-Trifluoromethyl Bond Activation Enables Arene C-H Trifluoromethylation. *Angew. Chem. Int. Ed* **2018**, *57*, 1311-1315.
36. Harris, C. F.; Bayless, M. B.; van Leest, N. P.; Bruch, Q. J.; Livesay, B. N.; Bacsa, J.; Hardcastle, K. I.; Shores, M. P.; de Bruin, B.; Soper, J. D., Redox-Active Bis(phenolate) N-Heterocyclic Carbene [OCO] Pincer Ligands Support Cobalt Electron Transfer Series Spanning Four Oxidation States. *Inorg. Chem.* **2017**, *56*, 12421-12435.
37. Yang, J. J.; Kirchmeier, R. L.; Shreeve, J. M., New electrophilic trifluoromethylating agents. *J. Org. Chem.* **1998**, *63*, 2656-2660.
38. Eisenberger, P.; Gischig, S.; Togni, A., Novel 10-I-3 hypervalent iodine-based compounds for electrophilic trifluoromethylation. *Chem.–Eur. J.* **2006**, *12*, 2579-2586.
39. Kieltsch, I.; Eisenberger, P.; Togni, A., Mild electrophilic trifluoromethylation of carbon- and sulfur-centered nucleophiles by a hypervalent iodine(III)-CF<sub>3</sub> reagent. *Angew. Chem. Int. Ed* **2007**, *46*, 754-757.
40. Matsnev, A.; Noritake, S.; Nomura, Y.; Tokunaga, E.; Nakamura, S.; Shibata, N., Efficient Access to Extended Yagupolskii-Umemoto-Type Reagents: Triflic Acid Catalyzed Intramolecular Cyclization of ortho-Ethynylaryltrifluoromethylsulfanes. *Angew. Chem. Int. Ed* **2010**, *49*, 572-576.
41. Liang, T.; Neumann, C. N.; Ritter, T., Introduction of Fluorine and Fluorine-Containing Functional Groups. *Angew. Chem. Int. Ed* **2013**, *52*, 8214-8264.
42. Beatty, J. W.; Douglas, J. J.; Cole, K. P.; Stephenson, C. R. J., A scalable and operationally simple radical trifluoromethylation. *Nature Communications* **2015**, *6*.
43. Jacquet, J.; Blanchard, S.; Derat, E.; Desage-El Murr, M.; Fensterbank, L., Redox-ligand sustains controlled generation of CF<sub>3</sub> radicals by well-defined copper complex. *Chemical Science* **2016**, *7*, 2030-2036.
44. Meucci, E. A.; Nguyen, S. N.; Camasso, N. M.; Chong, E.; Ariafard, A.; Canty, A. J.; Sanford, M. S., Nickel(IV)-Catalyzed C-H Trifluoromethylation of (Hetero)arenes. *J. Am. Chem. Soc.* **2019**, *141*, 12872-12879.

45. King, H. F.; Stanton, R. E.; Kim, H.; Wyatt, R. E.; Parr, R. G., Corresponding Orbitals and the Nonorthogonality Problem in Molecular Quantum Mechanics. *J. Chem. Phys.* **2004**, *47*, 1936-1941.
46. Neese, F., Definition of corresponding orbitals and the diradical character in broken symmetry DFT calculations on spin coupled systems. *J. Phys. Chem. Solids* **2004**, *65*, 781-785.
47. Dang, T. T.; Boeck, F.; Hintermann, L., Hidden Bronsted Acid Catalysis: Pathways of Accidental or Deliberate Generation of Triflic Acid from Metal Triflates. *J. Org. Chem.* **2011**, *76*, 9353-9361.
48. Wang, B.; Xiong, D.-C.; Ye, X.-S., Direct C–H Trifluoromethylation of Glycals by Photoredox Catalysis. *Org. Lett.* **2015**, *17*, 5698-5701.
49. Wang, S.-M.; Han, J.-B.; Zhang, C.-P.; Qin, H.-L.; Xiao, J.-C., An overview of reductive trifluoromethylation reactions using electrophilic '+CF<sub>3</sub>' reagents. *Tetrahedron* **2015**, *71*, 7949-7976.
50. Deolka, S.; Govindarajan, R.; Khaskin, E.; Fayzullin, R. R.; Roy, M. C.; Khusnutdinova, J. R., Photoinduced Trifluoromethylation of Arenes and Heteroarenes Catalyzed by High-Valent Nickel Complexes. *Angew. Chem. Int. Ed* **2021**, *60*, 24620-24629.
51. Koike, T.; Akita, M., Fine Design of Photoredox Systems for Catalytic Fluoromethylation of Carbon–Carbon Multiple Bonds. *Acc. Chem. Res.* **2016**, *49*, 1937-1945.
52. Mizuta, S.; Verhoog, S.; Wang, X.; Shibata, N.; Gouverneur, V.; Médebielle, M., Redox chemistry of trifluoromethyl sulfonium salts as CF<sub>3</sub> radical sources. *J. Fluorine Chem.* **2013**, *155*, 124-131.
53. Spell, M. L.; Deveaux, K.; Bresnahan, C. G.; Bernard, B. L.; Sheffield, W.; Kumar, R.; Ragains, J. R., A Visible-Light-Promoted O-Glycosylation with a Thioglycoside Donor. *Angew. Chem. Int. Ed.* **2016**, *55*, 6515-6519.
54. Egami, H.; Ito, Y.; Ide, T.; Masuda, S.; Hamashima, Y., Simple Photo-Induced Trifluoromethylation of Aromatic Rings. *Synthesis* **2018**, *50*, 2948-2953.
55. Al-Degs, Y. S.; Al-Ghouti, M. A., Influence of diesel acidification on dibenzothiophene removal: A new desulfurization practice. *Sep. Purif. Technol.* **2015**, *139*, 1-4.
56. Fulmer, G. R.; Miller, A. J. M.; Sherden, N. H.; Gottlieb, H. E.; Nudelman, A.; Stoltz, B. M.; Bercaw, J. E.; Goldberg, K. I., NMR Chemical Shifts of Trace Impurities: Common Laboratory Solvents, Organics, and Gases in Deuterated Solvents Relevant to the Organometallic Chemist. *Organometallics* **2010**, *29*, 2176-2179.

57. Evans, D. F., The Determination of the Paramagnetic Susceptibility of Substances in Solution by Nuclear Magnetic Resonance. *J. Chem. Soc.* **1959**, 2003-2005.
58. Piguet, C., Paramagnetic susceptibility by NMR: The "solvent correction" removed for large paramagnetic molecules. *J. Chem. Educ.* **1997**, *74*, 815-816.
59. Tyrra, W. E., Oxidative perfluoroorganylation methods in group 12-16 chemistry - The reactions of haloperfluoroorganics and In and InBr, a convenient new route to AgRf (R-f = CF<sub>3</sub>, C<sub>6</sub>F<sub>5</sub>) and reactions of AgRf with group 12-16 elements. *J. Fluorine Chem.* **2001**, *112*, 149-152.
60. Tanabe, Y.; Matsuo, N.; Ohno, N., Direct Perfluoroalkylation Including Trifluoromethylation of Aromatics with Perfluoro Carboxylic-Acids Mediated by Xenon Difluoride. *J. Org. Chem.* **1988**, *53*, 4582-4585.
61. Ong, J.; Loke, J. W. L.; Koh, H. L.; Fan, W. Y., Proflavine-catalysed trifluoromethylation of  $\alpha,\beta$ -unsaturated carbonyls. *Molecular Catalysis* **2022**, 530.
62. Singh, K.; Singh, R.; Hazari, A. S.; Adhikari, D., Bimodal photocatalytic behaviour of a zinc beta-diketiminato: application to trifluoromethylation reactions. *Chem. Commun.* **2022**, *58*, 4384-4387.
63. Neese, F., "The ORCA program System". *Wiley Interdisciplinary Reviews: Computational Molecular Science* **2012**, *2*, 73-78.
64. Neese, F., Software update: the ORCA program system, version 4.0. *Wiley Interdisciplinary Reviews: Computational Molecular Science* **2017**, *8*, e1327.
65. Perdew, J. P., Density-Functional Approximation for the Correlation-Energy of the Inhomogeneous Electron-Gas. *Physical Review B* **1986**, *33*, 8822-8824.
66. Becke, A. D., Density-Functional Exchange-Energy Approximation with Correct Asymptotic-Behavior. *Physical Review A* **1988**, *38*, 3098-3100.
67. Weigend, F.; Haser, M.; Patzelt, H.; Ahlrichs, R., RI-MP2: optimized auxiliary basis sets and demonstration of efficiency. *Chem. Phys. Lett.* **1998**, *294*, 143-152.
68. Weigend, F.; Ahlrichs, R., Balanced basis sets of split valence, triple zeta valence and quadruple zeta valence quality for H to Rn: Design and assessment of accuracy. *Physical Chemistry Chemical Physics* **2005**, *7*, 3297-3305.